Advection diffusion in nonchaotic closed flows: Non-Hermitian operators, universality, and localization

M. Giona,* V. Vitacolonna, S. Cerbelli, and A. Adrover
Dipartimento di Ingegneria Chimica, Università di Roma "La Sapienza," via Eudossiana 18, 00184 Roma, Italy
(Received 15 December 2003; revised manuscript received 5 May 2004; published 29 October 2004)

The qualitative spectral properties characterizing the advection-diffusion operator in two-dimensional steady incompressible flows can be obtained from the analysis of simple model flows on the torus, the velocity field of which attains the simple expression $\mathbf{v}(\mathbf{x})=(0,v_y(x))$. For this class of simple flows, the advection-diffusion operator reduces to a one-dimensional Schrödinger operator in the presence of an imaginary potential, which shares some spectral analogies with non-Hermitian quantum operators (e.g., spectral invariance), and is characterized by eigenfunction localization. The latter property (i.e., eigenfunction localization) is strictly related to the occurrence of a universal scaling of the eigenvalue spectrum with the Peclet number, the scaling exponent of which depends exclusively on the local behavior of the potential close to its critical points. The analysis is extended to a class of unbounded non-Hermitian operators, which include the Laplacian and the biharmonic operators coupled to an imaginary potential as special cases.

DOI: 10.1103/PhysRevE.70.046224 PACS number(s): 05.45.−a, 83.50.Xa, 47.15.−x

I. INTRODUCTION

Dispersion dynamics of passive scalars is a central issue in fluid dynamics and in many applied fields: environmental sciences (pollutant dispersion) [1], chemical engineering (mixing and chemical reaction in stirred vessels) [2,3], etc. Under the assumption that the velocity field is incompressible (i.e., $\boldsymbol{\nabla}\cdot\mathbf{v}=0$), dispersion is mathematically described by the advection-diffusion equation (ADE) which, in dimensionless form, attains the expression:

$$\frac{\partial\phi}{\partial t}=-\mathbf{v}\cdot\boldsymbol{\nabla}\phi+\varepsilon\boldsymbol{\nabla}^2\phi, \tag{1.1}$$

where $\varepsilon=\mathrm{Pe}^{-1}$ is the reciprocal of the Peclet number $\mathrm{Pe}=V_cL/D$ (V_c, L being characteristic velocity and length for the system, and D being the diffusivity). The Peclet number represents the ratio of the characteristic time of diffusion to that of advection.

Equation (1.1) has been analyzed for different classes of velocity fields: open [4–6] and closed [7–10] flows, and for families of flows possessing different kinematic features (nonchaotic, partially chaotic, and globally chaotic flows).

The nature of the flow domain (i.e., whether it is bounded or not) influences the way dispersion features must be considered and quantified. In unbounded flows, dispersion corresponds to the propagation of an initial disturbance by the simultaneous action of a given velocity field and diffusion. In this case, dispersion dynamics can be conveniently recast in the form of a stochastic Langevin equation. Consequently, dispersion properties can be described by means of statistical indicators (such as the mean square displacement) or, equivalently, through the scaling of the effective diffusivity tensor as a function of the molecular diffusivity. It has been shown that the long-time, long-distance dynamics of the solutions of Eq. (1.1) in unbounded domains approaches that associated with a pure diffusion equation with constant tensor diffusivity [11] (see also [12]). This result stems from the application of perturbation and asymptotic analysis [13] to Eq. (1.1).

In the study of dispersion in closed (bounded) flows, the analogy between Eq. (1.1) and stochastic differential equations is less useful, since all the statistical indicators, such as the mean square displacement, saturate asymptotically toward a constant value which is related to the finite size of the domain. Consequently, the quantitative description of dispersion in closed flows should be focused on how advection will eventually modify and enhance the rate at which equilibrium is approached with respect to the case where diffusion is the only transport mechanism operating.

It follows from the above observation that the mathematical description of dispersion in unbounded and closed flows is intrinsically different. It is grounded on asymptotic analysis and stochastic methods for open flows, while it is centered on the spectral (eigenvalue/eigenfunction) characterization in bounded domain (since the eigenvalues of the advection/diffusion operator correspond to the intrinsic rates of homogenization, and its eigenfunctions to the spatial patterns that will eventually appear).

Several authors have analyzed the qualitative features of homogenization in bounded domain in the presence of complex flow protocols yielding Lagrangian chaos [7–10]. Different scaling exponents of the eigenvalues with the Pe number have been observed and qualitatively associated with the kinematic features of the stirring protocol.

The present paper deals with a relatively simpler class of flows (two-dimensional autonomous), in the presence of deterministic velocity fields, for which the theoretical aspects of homogenization need to be clarified. Specifically, we analyze first a subclass of these flows, namely, the model flows on the two-dimensional torus for which $\mathbf{v}=(0,v_y(x))$ (which can be referred to as parallel flows), and subsequently we show that the spectral results obtained for these model flows

*Author to whom correspondence should be addressed.
Email address: max@giona.ing.uniromal.it

can be used to predict the scaling behavior of generic two-dimensional autonomous flows. The latter claim is supported by an extensive analysis of typical two-dimensional flow structures.

Stemming from the spectral structure of the ADE in this class of flows (parallel flows), a connection between between homogenization dynamics and non-Hermitian quantum mechanics is also discussed. We show that there exists a close analogy between Eq. (1.1) and the Schrödinger equation in the presence of an imaginary potential, and that, likewise the quantum analogous, homogenization is characterized by spectral invariance. Moreover, universal spectral scaling and eigenfunction localization are the other salient features characterizing the non-Hermitian operators associated with homogenization dynamics.

The paper is organized as follows. Section II introduces the concept of imaginary potential for parallel flows and describes the analogy with non-Hermitian quantum mechanics. Section III addresses the occurrence of universality and eigenfunction localization. Specifically, starting from the empirical observation of the eigenfunction localization, we prove that a universal scaling occurs in the behavior of the dominant eigenvalue as a function of the Peclet number, which is controlled exclusively by the local properties of the flow.

Finally, Sec. IV addresses how the spectral results and the universality properties can be applied to predict the spectral behavior of physically realizable flows (the cases of the cavity flow, the Couette flow, and of other model flows on the torus are addressed).

II. IMAGINARY POTENTIAL AND NON-HERMITIAN OPERATORS

Let us consider the advection-diffusion equation (1.1) driven by autonomous velocity fields $\mathbf{v}(\mathbf{x})$ in a closed two-dimensional domain $\mathcal{M}$ of the Euclidean plane. Since the normal component of the velocity field vanishes at the boundary $\partial\mathcal{M}$, Eq. (1.1) satisfies the boundary condition of Neumann type, namely the normal derivative of ϕ vanishes at $\partial\mathcal{M}$. Alternatively, a convenient prototype of flow domain of a spatially confined flow is the two-dimensional torus, i.e., $\mathcal{M}=\mathcal{I}^2$ where $\mathcal{I}^2$ is the unit square $\mathcal{I}^2=\{(x,y)\,|\,0\leqslant x,y\leqslant 1\}$, with opposite edges identified. Correspondingly, Eq. (1.1), defined in $\mathcal{I}^2$, is equipped with periodic boundary conditions.

Theoretical results from the theory of linear operator [14,15] ensure that the advection-diffusion operator

$$\mathcal{L} = -\mathbf{v}(\mathbf{x})\cdot\boldsymbol{\nabla} + \varepsilon\boldsymbol{\nabla}^2 \tag{2.1}$$

possesses the following properties: (i) it admits a countable set of separated eigenvalues, (ii) the corresponding eigenfunctions form a complete basis in the space of square summable functions in $\mathcal{M}$, fulfilling either Neumann or periodicity conditions (see above), (iii) all of the eigenvalues (with the exception of the zero eigenvalue corresponding to the constant eigenfunction) possess negative real part (throughout this paper we use the symbol λ_n to indicate the real part of the eigenvalues with reversed sign).

Throughout this section we consider, a simple model for an incompressible flow, which attains the structure

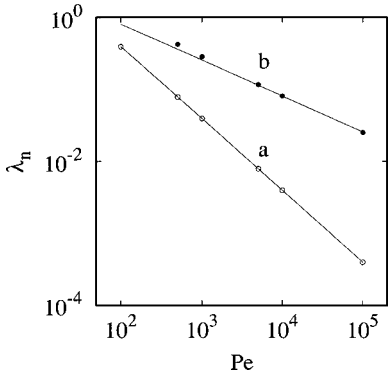

FIG. 1. Real part with reversed sign λ_n of the dominant eigenvalues of the diffusive and convective branch as a function of Pe for the ASF. Line (a) and (○) refer to the diffusive branch, line (b) and (●) to the convection-enhanced branch.

$$\mathbf{v}(\mathbf{x}) = (0, v_y(x)) \tag{2.2}$$

with a single nonvanishing component of the velocity field which, due to incompressibility, depends solely on the other coordinate. These model flows can be referred to as *parallel flows* on the torus.

The autonomous sine-flow (ASF), defined by $v_y(x)=\sin(2\pi x)$ belongs to this class, and has been widely investigated in the literature [16,17]. Its eigenvalue spectrum possesses two branches (see Fig. 1): a diffusive branch, characterized by real eigenvalues, for which the λ_n's are proportional to ε, i.e., $\lambda_n \sim \mathrm{Pe}^{-1}$, and a *convection-enhanced* branch, for which λ_n's are proportional to the square root of ε, i.e., $\lambda_n \sim 1/\sqrt{\mathrm{Pe}}$. The dominant eigenvalue (i.e., the eigenvalue possessing the smallest λ_n) belongs to the diffusive branch, and the structure of the corresponding eigenfunction closely resembles that of the streamfunction as $\varepsilon \to 0$.

The aim of the next two sections is to analyze in detail the spectral properties of parallel flows.

A. Imaginary potentials

Let us consider the class of flows defined by Eq. (2.2) in $\mathcal{I}^2$, the ASF being a particular example of this class. The advection-diffusion operator for these flows attains the form

$$\mathcal{L}[\phi](\mathbf{x}) = -v_y(x)\frac{\partial\phi}{\partial y} + \varepsilon\left(\frac{\partial^2\phi}{\partial x^2} + \frac{\partial^2\phi}{\partial y^2}\right). \tag{2.3}$$

By introducing the function $\psi(x,t)$ defined by

$$\phi(\mathbf{x},t) = e^{-i2\pi my - \varepsilon 4\pi^2 m^2 t}\psi(x,t) \tag{2.4}$$

where m is an integer and $i=\sqrt{-1}$, the ADE becomes

$$\frac{\partial\psi}{\partial t} = i2\pi m v_y(x)\psi + \varepsilon\frac{\partial^2\psi}{\partial x^2}. \tag{2.5}$$

Therefore, homogenization dynamics described by Eq. (1.1) on the unit square reduces to a countable family of second-order differential problems on the unit interval]0,1[equipped with periodic boundary conditions, defined by the evolution operators $\mathcal{A}_m[\psi]=iV_m(x)\psi+\varepsilon\, d^2\psi/dx^2$, where

$V_m(x)=2\pi m v_y(x)$. The case $m=0$ gives rise to real eigenvalues, which are the eigenvalues of the diffusion operator $-\varepsilon 4\pi^2 n^2$, $n=0,1,\ldots$, and constitute the diffusive branch of the eigenvalue spectrum of the advection-diffusion operator. Apart from the diffusive branch, the spectral properties of the ADE and the analysis of the origin of the scaling behavior characterizing the convection-enhanced branch, can be obtained from the analysis of the operator:

$$\mathcal{A}[\psi] = \varepsilon \frac{d^2\psi}{dx^2} + iV(x)\psi, \tag{2.6}$$

where $V(x)=V_1(x)$, which can be viewed as a second-order non-Hermitian Schrödinger operator in the presence of an imaginary potential. More precisely, let $\{\nu_{m,n}(\varepsilon)\}$, $m=\ldots, -1,0,1,\ldots$, $n=1,2,\ldots$ be the eigenvalues of $\mathcal{L}$ defined by Eq. (2.3), $\{\mu_n(\varepsilon)\}$ the eigenvalues of $\mathcal{A}$ defined by Eq. (2.6), respectively, and $\{\phi_{m,n}(x,y)\}$, $\{\psi_m(x)\}$ the corresponding systems of eigenfunctions. We have

$$\lambda_{m,n}(\varepsilon) = m\mu_n(\varepsilon/m) - \varepsilon 4\pi^2 m^2 \tag{2.7}$$

and

$$\phi_{m,n}(x,y) = e^{-i2\pi my}\psi_n(x). \tag{2.8}$$

Due to the close relationship between the advection-diffusion operator Eq. (2.3) and the operator $\mathcal{A}$ defined by Eq. (2.6), we will refer to $iV(x)$ as "the imaginary potential generating the flow," although we stress out that this potential has nothing to do with the classical concept of velocity potential adopted in fluid dynamics [18].

B. Generalized non-Hermitian operators

In order to analyze the spectral structure of the operator $\mathcal{A}$ associated with the ADE, and to define properly its universality properties (see Sec. III), let us consider a slight generalization of it, by defining the class of differential operators of increasing orders $2q$, $q=1,2,\ldots$ associated with an imaginary potential, as

$$\mathcal{A}_q[\psi] = (-1)^{q-1}\varepsilon D_x^{2q}\psi + iV(x)\psi, \quad q=1,2,\ldots, \tag{2.9}$$

where $D_x^n = d^n/dx^n$. For $q=1$, Eq. (2.6) is recovered, while the case $q=2$ corresponds to a relaxation dynamics driven by a biharmonic operator.

The family of operators $\mathcal{A}_q$ is defined in the functional space $L^2_{\mathrm{per}}(]0,1[)$ of square summable complex-valued periodic functions in the unit interval $]0,1[$. This functional space is a Hilbert space, equipped with the inner product

$$(f,g) = \int_0^1 f(x)\overline{g}(x)dx, \quad f,g \in L^2_{\mathrm{per}}(]0,1[). \tag{2.10}$$

We denote with $\|\cdot\|_{L^2}$ the norm inherited by it, namely $\|f\|_{L^2} = (f,f)^{1/2}$. We use the notation $\overline{g}$ to indicate the complex conjugate of g.

By choosing the natural basis of periodic functions $\{e^{i2\pi kx}\}_{k=-\infty}^{\infty}$, the action of the operator $\mathcal{A}_q$ on a function $\psi \in L^2_{\mathrm{per}}(]0,1[)$, $\mathcal{A}_q[\psi]=f$ is expressed by the relation:

$$f_n = -(2\pi n)^{2q}\psi_n + i\sum_m V_{n-m}\psi_m, \tag{2.11}$$

where f_n, ψ_n, and V_n are the Fourier coefficients of $f(x)$, $\psi(x)$, and $V(x)$, respectively. In the particular case of a sinusoidal potential (corresponding to the ASF), Eq. (2.11) become

$$f_n = -(2\pi n)^{2q}\psi_n + 2\pi(\psi_{n-1} - \psi_{n+1}). \tag{2.12}$$

Thus, for the ASF potential, the matrix representation of the operator $\mathcal{A}_q$ attains a tridiagonal form, which, for $q=1$ resembles that of a non-Hermitian Schrödinger equation in the presence of a tight binding potential (e.g., deriving from a imaginary vector potential associated with the action of a magnetic field on a quantum particle). This problem leads to a non-Hermitian second-order operator, characterized by an almost tridiagonal matrix representation [19–21]. However, there are differences and similarities between these two problems. The differences are related to the properties of the entries of the upper and lower diagonals. In the non-Hermitian quantum mechanical problem, the entries of these diagonals are arbitrary positive values, while in the ASF problem, the entries are equal within each subdiagonal, and possess opposite sign when considering elements belonging to different subdiagonals. The analogy between the two problems refers to the global spectral features, namely spectral invariance, that is discussed in detail in Sec. III.

C. Properties of the eigenvalues

In this section, we derive some relations for the eigenvalues of the operator $\mathcal{A}_q$, that will be useful in the analysis of its global properties (Sec. IV). Let $\mu=\mu_R+i\omega$ be an eigenvalue of $\mathcal{A}_q$, and $\psi(x)$ its eigenfunction:

$$(-1)^{q-1}\varepsilon D_x^{2q}\psi(x) + iV(x)\psi(x) = \mu\psi(x). \tag{2.13}$$

By multiplying Eq. (2.13) by $\overline{\psi}$ and integrating over the unit interval, one obtains

$$(-1)^{q-1}\varepsilon(D_x^{2q}\psi,\psi) + i(V\psi,\psi) = \mu\|\psi\|_{L^2}. \tag{2.14}$$

Since $(D_x^{2q}\psi,\psi) = -(D_x^{2q-1}\psi, D_x\psi)$, by iterating the integration-by-parts procedure one finally obtains

$$-\varepsilon\|D_x^q\psi\|_{L^2}^2 + i(V\psi,\psi) = \mu\|\psi\|_{L^2}^2, \tag{2.15}$$

which indicates that the real and imaginary parts of the eigenvalues attain the expressions

$$\mu_R = -\frac{\varepsilon\|D_x^q\psi\|_{L^2}^2}{\|\psi\|_{L^2}^2}, \tag{2.16}$$

$$\omega = \frac{(V\psi,\psi)}{\|\psi\|_{L^2}^2}. \tag{2.17}$$

Equation (2.16) shows that all the eigenvalues of $\mathcal{A}_q$ possess negative real part, i.e., that $\mathcal{A}_q$ is a dissipative operator. An

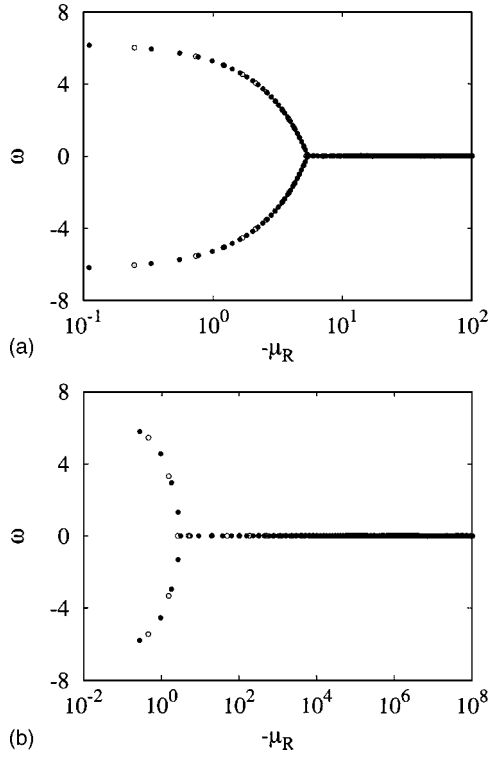

FIG. 2. Spectral plots $-\mu_R$-ω of $\mathcal{A}_q$ for $V(x)=2\pi\sin(2\pi x)$ showing spectral invariance. The tail of the eigenvalue spectrum diverging to infinity along the real line is not shown for enhancing visualization of the forklike structure. (a) $q=1$ (Laplacian operator) (○) refers to $\mathrm{Pe}=10^3$, (●) to $\mathrm{Pe}=5\times10^3$. (b) $q=1$ (Biharmonic operator) (○) refers to $\mathrm{Pe}=2\times10^4$, (●) to $\mathrm{Pe}=10^5$.

alternative expression for the eigenvalues stems from the integration of Eq. (2.13) over the unit interval:

$$(-1)^{q-1}\varepsilon\int_0^1 D_x^{2q}\psi(x)dx + i\int_0^1 V(x)\psi(x)dx = \mu\int_0^1 \psi(x)dx. \tag{2.18}$$

By enforcing the periodicity of ψ, the first integral at the left-hand side of Eq. (2.18), namely $(D_x^{2q}\psi(x),1)$, vanishes so that Eq. (2.18) reduces to

$$\mu\int_0^1 \psi(x)dx = i\int_0^1 V(x)\psi(x)dx, \tag{2.19}$$

which can be expressed in a more compact form as $\mu = i(\psi,V)/(\psi,1)$. Equations (2.16), (2.17), and (2.19) are useful expressions which relate the eigenvalues to the norms and scalar products of the corresponding eigenfunctions. These expressions will be used in the next section to prove some scaling properties of the eigenvalues.

III. LOCALIZATION AND UNIVERSALITY

A. Spectral invariance

A first qualitative property characterizing the eigenvalue spectrum of the operators $\mathcal{A}_q$ is its *spectral invariance*. To clarify this concept, let us consider the spectral plots of the operators $\mathcal{A}_q$, i.e., the graphical representation of the eigenvalues in the μ_R-ω plot. By spectral invariance we mean the following property: the eigenvalues of $\mathcal{A}_q$ for fixed q, taking ε as parameter, lie, at small values of ε, onto a single smooth master set which is the union of a finite number of curve arcs. This phenomenon is illustrated in Figs. 2(a) and 2(b) for $V(x)=2\pi\sin(2\pi x)$ (the ASF potential) for $q=1$ and $q=2$, respectively. These plots show the occurrence of a pitchfork-like set which is a characteristic feature of the spectral plot of $\mathcal{A}_q$ independently of q in the presence of a sinusoidal imaginary potential.

A similar phenomenon has been observed by Hatano and Nelson [19,20] for non-Hermitian quantum operators and has been addressed further by Goldshein and Khoruzhenko [21] for random matrices arising from the physics of magnetic flux lines.

The inspection of the spectral plots depicted in Fig. 2 permits to infer the following observations about the spectrum of $\mathcal{A}_q$. The spectrum is composed by both complex and real eigenvalues. It is symmetric around the μ_R axis, which means that for any complex eigenvalue μ, its complex conjugate $\overline{\mu}$ belongs to the spectrum. This property is related to the symmetries of the potential (see the discussion in Sec. III D). The dominant eigenvalue (i.e., the eigenvalue possessing the smallest real part in absolute value) is complex and its real part approaches 0 as $\varepsilon\to0$. Conversely, at large Pe numbers, its imaginary part approaches 2π.

These properties are explained in the next section as a consequence of eigenfunction localization, which implies several other results, among which the occurrence of an universal scaling law for the real part of the eigenvalue with respect to the Peclet number.

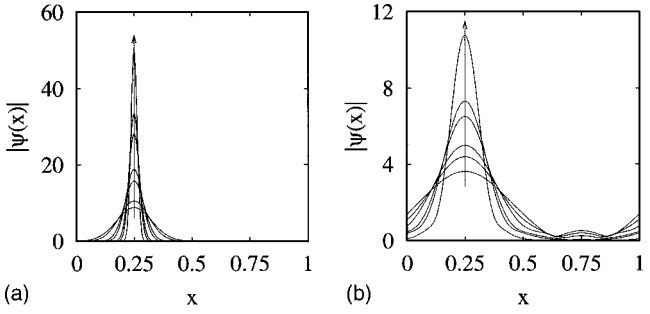

FIG. 3. Dominant eigenfunction $|\psi(x)|$ vs x for $\mathcal{A}_q$ in the presence of the ASF potential for several values of the Peclet number $\mathrm{Pe}=\varepsilon^{-1}$. (a) $q=1$. $\mathrm{Pe}=5\times10^2$, 10^3, 5×10^3, 10^4, 5×10^4, 10^5, 5×10^5. (b) $q=2$. $\mathrm{Pe}=2\times10^3$, 5×10^3, 10^4, 5×10^4, 10^5, 10^6. The arrows indicate increasing values of Pe.

B. Eigenfunction localization

Let us consider again the sinusoidal potential $V(x)=2\pi\sin(2\pi x)$ and the behavior of the dominant eigenfunctions. Figures 3(a) and 3(b) show the behavior of the

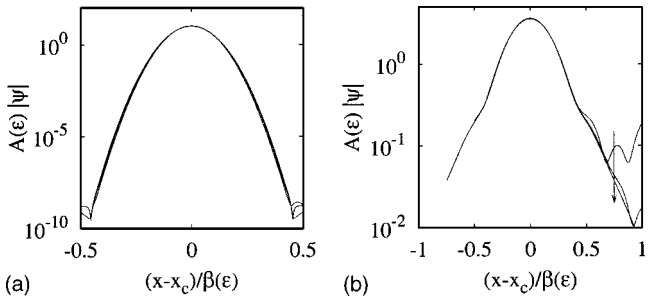

FIG. 4. Rescaling of the dominant eigenfunction into a single master curve $A(\varepsilon)|\psi_\varepsilon(x)|$ vs $(x-x_c)/\beta(\varepsilon)$. (a) Operator $\mathcal{A}_1$. Three values of $\mathrm{Pe}=10^4$, 10^5, 10^6 are depicted. (b) Operator $\mathcal{A}_2$. Three values of $\mathrm{Pe}=2\times10^4$, 10^5, 10^6 are depicted. The arrow indicates increasing values of Pe.

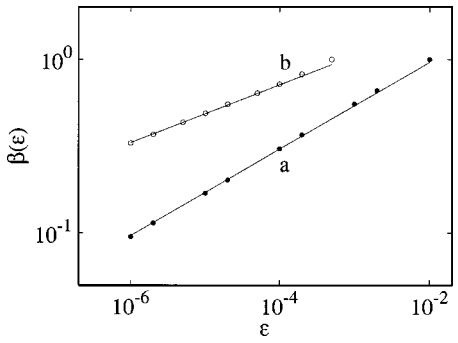

FIG. 5. Boundary-layer width $\beta(\varepsilon)$ vs $\varepsilon=\mathrm{Pe}^{-1}$. Filled dots (●) refers to $\mathcal{A}_1$, open circles (○) to $\mathcal{A}_2$. Line (a) is the scaling $\beta(\varepsilon)\sim\varepsilon^{1/4}$, line (b) is $\beta(\varepsilon)\sim\varepsilon^{1/6}$.

modulus $|\psi(x)|$ of the dominant eigenfunction[1] $\psi(x)$ for different values of the Peclet number (i.e., of ε) for the operators $\mathcal{A}_1$ [Fig. 3(a)], and $\mathcal{A}_2$ [Fig. 3(b)]. The dominant eigenfunction is localized around the critical point $x=1/4$, which corresponds to the local maximum of the potential (due to the symmetry of the potential, the eigenfunction associated with the complex-conjugate eigenvalue is localized around the local minimum at $x=3/4$, see Sec. III D).

Henceforth, we will indicate with the notation $\psi_\varepsilon(x)$ an eigenfunction of the generalized non-Hermitian operator $\mathcal{A}_q$ for a fixed value ε of the parameter corresponding to the reciprocal of the Peclet number. The family of dominant eigenfunctions, parametrized with respect to ε, can be rescaled into a single master curve $g(\xi)$, by considering the following scaling relation:

$$\psi_\varepsilon(x)=A^{-1}(\varepsilon)g\left(\frac{x-x_c}{\beta(\varepsilon)}\right), \tag{3.1}$$

where $x_c=1/4$, $\beta(\varepsilon)$ is the scaling factor and $A(\varepsilon)=\beta(\varepsilon)$ a normalization factor. Figures 4(a) and 4(b) show the results of the normalization Eq. (3.1) for the two families of dominant eigenfunctions depicted in Fig. 3. The physical meaning of $\beta(\varepsilon)$ is essentially the "boundary-layer width" within which the eigenfunctions are localized. This quantity follows a power-law scaling with ε, $\beta(\varepsilon)\sim\varepsilon^{1/4}$, see Fig. 5, for the second-order operator $\mathcal{A}_1$, while $\beta(\varepsilon)\sim\varepsilon^{1/6}$ for the fourth-order operator $\mathcal{A}_2$. A theory justifying the occurrence of this scaling law is developed in the next section in the more general framework of spectral universality exhibited by this class of non-Hermitian operators.

Let us complete the phenomenological description of the eigenfunction properties. Eigenfunction localization around the potential extrema (critical points) characterizes the family of eigenfunctions associated with complex eigenvalues. To give an example, Figs. 6(a)–6(c) depict the shape of the first three dominant eigenfunctions associated with complex eigenvalues for $\mathrm{Pe}=10^4$. The eigenfunctions are ordered in an increasing way with respect to the absolute value of the real part. All of these eigenfunctions display localization around $x_c=1/4$ and, as the order increases, the occurrence of multiple local maxima/minima. Due to the symmetry of the potential, for each eigenvalue μ, its complex conjugate belongs to the spectrum. Since the eigenfunction associated with $\overline{\mu}$, can be obtained by symmetry from the eigenfunction associated with μ (see Sec. III D), the plot of these eigenfunctions has not been reported.

Due to the splitting of the eigenvalue spectrum into a real and complex branches, which makes the spectral plots to attain a typical forklike structure, there exist eigenfunctions of $\mathcal{A}_q$ associated with real eigenvalues. Numerical simulations indicate that the eigenfunctions belonging to the real part of the spectrum are not localized.

C. Universality in the eigenvalue spectra

Eigenfunction localization and its rescaling onto a single master curve for $\varepsilon\to0$ (see Fig. 4) is a manifestation of a fundamental physical property of the non-Hermitian operators $\mathcal{A}_q$, namely the universality of eigenvalue scaling with the Peclet number. By assuming the localization rescaling[2] Eq. (3.1), we derive its functional implications as it regards the behavior of the dominant eigenvalue with ε.

It is convenient to consider first a particular family of symmetric potentials, and to extend subsequently the implications of the results obtained for generic $V(x)$. The class of potentials considered is characterized by the following properties: (i) $V(x)$ is continuous and possesses generalized derivative in $]0,1[$; (ii) $V(x)=-V(1-x)$; (iii) $V(0)=0$; (iv) $V(x)$ is unimodal in $]0,1/2[$. Therefore, this class of potentials shows the occurrence of a single local maximum at $x=x_m$,

[1]Spectral analysis was performed by expanding the eigenvalue problem $\mathcal{A}_q[\psi]=\mu\psi$ in Fourier series. The number of Fourier modes $\{e^{2\pi ikx}\}_{k=-N}^{N}$ adopted in the spectral analysis varies with the Peclet number, in order to ensure numerical accuracy: we consider $N=100$ for low Peclet values $\mathrm{Pe}=10^2-10^3$, up to $N=1600$ for $\mathrm{Pe}=10^6$. The eigenfunctions depicted in Fig. 3 are normalized to unit L^1 norm.

[2]It is worth pointing out, that eigenfunction localization represents an empirical finding, while the rest of the analysis, namely the universal scaling, derives from it, and from the functional relations Eqs. (2.16) and (2.19).

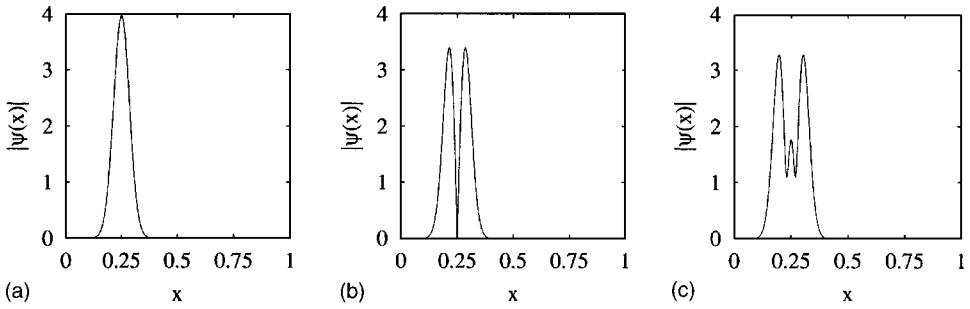

FIG. 6. Modulus $|\psi(x)|$ of the first three dominant eigenfunctions [from (a) to (c)] of the operator $\mathcal{A}_1$ in the presence of the sinusoidal (ASF) potential $V(x)=2\pi\sin(2\pi x)$.

and a single local minimum at x_m'. By the properties of $V(x)$ it follows that $x_m=1-x_m'$ and $V(x_m')=-V(x_m)$.

Let us indicate with $V_{\rm per}(x)$ the periodicization of a generic potential $V(x)$ over the real line. Since the spectral properties are invariant under translations of the potential, i.e., the operators $\mathcal{A}_q$ and $\tilde{\mathcal{A}}_q$ associated with $V(x)$ and $\tilde{V}(x)=V(x-a)$ where a is a real number, possess identical eigenvalue spectra, instead of the potential $V(x)$, we may always consider the translated potential $\tilde{V}(x)=V_{\rm per}(x-x_m)$. This observation is made exclusively in order to simplify the notation by translating the critical point at the origin, so that the expression for the series expansion of the potential near the critical point attain a simpler form.

The potential $\tilde{V}(x)$ possesses the maximum at $x=0$. Let us expands $V(x)$ near its local maximum

$$\tilde{V}(x)=V_M-V_1|x|^\gamma+o(|x|^\gamma), \tag{3.2}$$

where γ is the nonlinearity exponent characterizing the behavior of the potential near the critical point. In the case of the sine-flow potential $\gamma=2$, since this potential possesses a quadratic nonlinearity in the neighborhood of the critical point. Throughout this section, we keep using the notation $\mathcal{A}_q$ to indicate the operator Eq. (2.9) associated with the translated potential $\tilde{V}$.

Let $\mu(\varepsilon)$ and $\psi_\varepsilon(x)$ be the dominant eigenvalue and the associated eigenfunction for the operator $\mathcal{A}_q$ for a value ε of the parameter. Let us further assume the validity of Eq. (3.1), i.e.,

$$\psi_\varepsilon(x)=A^{-1}(\varepsilon)g(\xi)|_{\xi=x/\beta(\varepsilon)}. \tag{3.3}$$

Before developing further the analysis it is important to point out that Eq. (3.3) does not imply any assumption on the functional form of $\beta(\varepsilon)$, other that it decays to zero as $\varepsilon\to 0$.

By substituting Eq. (3.3) into Eq. (2.16), and performing the change of variable $\xi=x/\beta(\varepsilon)$, it follows that

$$-\mu_R(\varepsilon)=\frac{\varepsilon}{\beta^{2q}(\varepsilon)}\frac{\int_{-1/2\beta(\varepsilon)}^{1/2\beta(\varepsilon)}|D_\xi^q g(\xi)|^2\,d\xi}{\int_{-1/2\beta(\varepsilon)}^{1/2\beta(\varepsilon)}|g(\xi)|^2\,d\xi}, \tag{3.4}$$

where $D_\xi g(\xi)=dg(\xi)/d\xi$. Since the function $g(\xi)$ is vanishingly small outside a narrow interval centered at $\xi=0$, and since for $\varepsilon\to 0$ the integration limits approach $\pm\infty$, Eq. (3.4) implies that

$$-\mu_R(\varepsilon)\simeq C\frac{\varepsilon}{\beta^{2q}(\varepsilon)}, \tag{3.5}$$

where $C=\int_{-\infty}^{\infty}|D^q g(\xi)|^2\,d\xi/\int_{-\infty}^{\infty}|g(\xi)|^2\,d\xi$ is a positive constant. We may use Eq. (2.19) to get an alternative expression for $\mu_R(\varepsilon)$. By enforcing Eq. (3.3) with $V(x)$ replaced by $\tilde{V}(x)$, and making the same approximations applied above for the integrals Eq. (3.4), as it regards the integration limits, one obtains

$$\mu(\varepsilon)\int_{-\infty}^{\infty}g(\xi)d\xi=i\int_{-\infty}^{\infty}\tilde{V}(\beta(\varepsilon))g(\xi)d\xi. \tag{3.6}$$

Owing to the fact that $g(\xi)$ is localized around $\xi=0$, the integral at the r.h.s. of Eq. (3.6) depends on the local behavior of $V(\beta(\varepsilon)\xi)$ near $\xi=0$. Therefore we can apply the local expansion Eq. (3.2), thus obtaining a linear system for the two unknowns $\mu_R(\varepsilon)$ and $\omega(\varepsilon)$,

$$\begin{bmatrix}A_{0,R} & -A_{0,I}\\ A_{0,I} & A_{0,R}\end{bmatrix}\begin{bmatrix}\mu_R(\varepsilon)\\ \omega(\varepsilon)\end{bmatrix}=\begin{bmatrix}-V_MA_{0,I}+V_1\beta^\gamma(\varepsilon)A_{1,I}\\ V_MA_{0,R}-V_1\beta^\gamma(\varepsilon)A_{1,R}\end{bmatrix}, \tag{3.7}$$

where

$$A_{0,k}=\int_{-\infty}^{\infty}g_k(\xi)d\xi,\quad A_{1,k}=\int_{-\infty}^{\infty}|\xi|^\gamma g_k(\xi)d\xi,\quad k=R,I \tag{3.8}$$

and $g(\xi)=g_R(\xi)+ig_I(\xi)$. The solution of the linear system (3.7) is:

$$-\mu_R(\varepsilon)=\beta^\gamma(\varepsilon)\frac{V_1(A_{0,I}A_{1,R}-A_{0,R}A_{1,I})}{A_{0,R}^2+A_{0,I}^2}, \tag{3.9}$$

$$\omega(\varepsilon)=V_M-\beta^\gamma(\varepsilon)\frac{V_1(A_{0,R}A_{1,R}+A_{0,I}A_{1,I})}{A_{0,R}^2+A_{0,I}^2}. \tag{3.10}$$

Let us first consider the scaling behavior of the eigenvalues with ε. By equating Eqs. (3.5) and (3.9) it follows that

$$\beta(\varepsilon)=B\varepsilon^{1/(2q+\gamma)}=B\varepsilon^\eta, \tag{3.11}$$

where B is a positive constant, and therefore from Eq. (3.5) one obtains

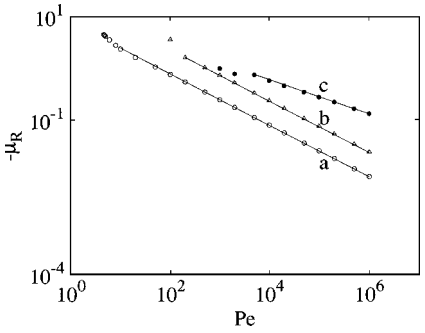

FIG. 7. Real part of the dominant eigenvalues $-\mu_R$ vs Pe for the operators $\mathcal{A}_q$ in the presence of the ASF potential. Open circles (○) $q=1$, dominant eigenvalue, (△) $q=1$ second dominant eigenvalue, (●) $q=2$ dominant eigenvalue. Lines (a) and (b) are the scaling $-\mu_R \sim \mathrm{Pe}^{-1/2}$, line (c) $-\mu_R \sim \mathrm{Pe}^{-1/3}$ as predicted by Eqs. (3.12) and (3.13).

$$-\mu_R(\varepsilon) \sim \varepsilon^{\alpha} \sim \mathrm{Pe}^{-\alpha}, \tag{3.12}$$

where the exponent α is given by

$$\alpha = \frac{\gamma}{2q+\gamma}. \tag{3.13}$$

Equation (3.13) is the main result regarding universality, since it expresses the scaling behavior of the dominant eigenvalue as a function of the local behavior near the critical point, and of the order $2q$ of the differential operator $\mathcal{A}_q$. In a similar way, Eq. (3.10) indicates that the imaginary part $\omega(\varepsilon)$ behaves for $\varepsilon \to 0$ as

$$|V_M - \omega(\varepsilon)| \sim \varepsilon^{\alpha} \sim \mathrm{Pe}^{-\alpha}, \tag{3.14}$$

i.e., it approaches V_M following a scaling law analogous to that one characterizing the real part.

Equations (3.12) and (3.13) predict that for $q=1$ and $\gamma=2$ (quadratic potential near the critical point), the real part of the dominant eigenvalue follows the scaling $-\mu_R \sim \mathrm{Pe}^{-1/2}$, which corresponds to the convection-enhanced regime. Conversely, for the fourth-order operator $\mathcal{A}_q$ with $q=2$, and with $V(x)$ quadratic near the critical point, Eqs. (3.12) and (3.13) yield $-\mu_R \sim \mathrm{Pe}^{-1/3}$. The comparison with the spectral results is depicted in Fig. 7, for $q=1, 2$, revealing the perfect agreement between theory and simulations. The power-law Eq. (3.12) characterizes the entire family of complex conjugate eigenvalues (corresponding to the two arms of the fork depicted in Fig. 2). This is shown in Fig. 7 [see lines (a) and (b)] for the first and second dominant eigenvalue.

It is important to observe that Eqs. (3.11)–(3.14) express a universality principle in the scaling of the spectral properties with ε (or Pe), for $\varepsilon \to 0$, since the scaling exponents (α and η) are not influenced by the fine details of the potential, but depend exclusively on the behavior near the critical point[3] (expressed by the exponent γ).

[3]In this exclusive meaning, these equations can be viewed as "analogous" to the Feigenbaum universality characterizing the period-doubling bifurcation for unimodal maps on the interval.

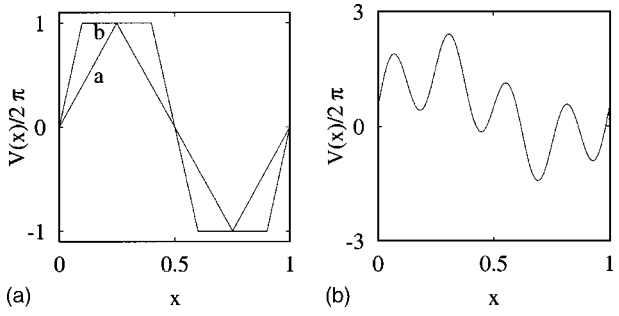

FIG. 8. (a) Potential $V(x)$ given by Eq. (3.16). Line (a) refers to $h=1/4$, line (b) to $h=0.1$. (b) Multimaxima potential $V(x)=2\pi[\sin(2\pi x)+0.5\sin(8\pi x)]$.

Equations (3.11)–(3.14) are the core of a *universality theory* for the spectral properties in homogenization dynamics (restricted to two-dimensional autonomous flows). This theory is grounded on the properties of three scaling exponents: the exponent η associated with the scaling of the boundary-layer width $\beta(\varepsilon)$ Eq. (3.11), the exponent α characterizing the decay of the real part of the dominant eigenvalue Eq. (3.12), and the exponent ξ which refers to the relaxation properties of the imaginary part toward V_M, $|V_M - \omega(\varepsilon)| \sim \varepsilon^{\kappa}$, Eq. (3.14). The relations between these three exponents are

$$\alpha = \gamma\eta, \qquad \kappa = \alpha. \tag{3.15}$$

In order to assess further the validity of Eq. (3.12), let us consider a family of trapezoidal potentials [see Fig. 8(a)]:

$$V(x) = \begin{cases} 2\pi x/h, & x \in]0,h[, \\ 2\pi, & x \in]h,1/2-h[, \\ \pi(1-2x)/h, & x \in]1/2-h,1/2+h[, \\ -2\pi, & x \in]1/2+h,1-h[, \\ 2\pi(x-1)/h, & x \in]1-h,1[, \end{cases} \tag{3.16}$$

where $h \in [0,1/4]$. The potentials Eq. (3.16) are continuous for any $h \in]0,1/4]$. For $h=1/4$, Eq. (3.16) yields a tent potential and therefore $\gamma=1$. For $h \to 0$, $V(x)$ approaches a discontinuous square-wave potential. In the "pathological" case of a potential $V(x)$ which possesses maxima and minima, in the neighborhood of which $V(x)$ is constant (flat critical points), the value $\gamma=\infty$ can be assigned to these critical points, since $\gamma=\infty$ can be viewed as the limit value for the exponents γ_n, $n=1,2,\ldots$ associated with an analytic sequences of potentials $V_n(x)$ converging to $V(x)$.

Therefore, for intermediate values of $h<1/4$, Eq. (3.16) yields a trapezoidal symmetric potential, which is flat near the critical point, thus $\gamma=\infty$. Equation (3.13) predicts the value $\alpha=1/3$ for $h=1/4$, $q=1$, while for any other value of h within the interval $[0,1/4[$, $\alpha=1$, i.e., the dominant eigenvalue scales "diffusively." Figure 9 depicts the behavior of $-\mu_R$ vs Pe for the operator $\mathcal{A}_1$ driven by the potential Eq. (3.16). For $h=1/4$ [line (a)] the scaling $-\mu_R \sim \mathrm{Pe}^{-1/3}$ is ob-

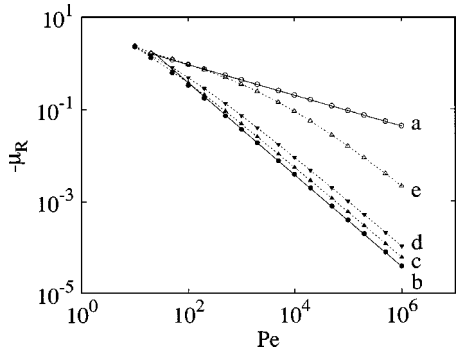

FIG. 9. Real part of the dominant eigenvalues $-\mu_R$ vs Pe for the operator $\mathcal{A}_1$ driven by the potential Eq. (3.16). Open circles (○) refer to the tent potential $h=1/4$, solid line (a) to the scaling $-\mu_R \sim \mathrm{Pe}^{-1/3}$ as predicted by Eqs. (3.12) and (3.13) with $\gamma=1$. Filled dots (●) to the square-wave potential $h=0$, solid line (b) to the scaling $-\mu_R \sim \mathrm{Pe}^{-1}$ as predicted by the theoretical scaling with $\gamma=\infty$. Lines (c)–(e) refer to the potential Eq. (3.16) for $h=0.05$, 0.10, and 0.2, respectively.

served, while for $h \to \infty$, corresponding to a square-wave discontinuous potential [line (b)], $-\mu_R \sim \mathrm{Pe}^{-1}$, as predicted by Eq. (3.13) for $\gamma \to \infty$. The behavior for intermediate values of h is particularly interesting. When h is small [$h=0.05$, line (c) in Fig. 9], the scaling of the real part of the dominant eigenvalue follows a power-law decay with an exponent $\alpha=1$. As h increases further [$h=0.1$, line (d) and $h=0.2$, line (e)], a crossover in the $-\mu_R$-Pe plot appears. This phenomenon is evident for $h=0.2$ [line (e)], which for $\mathrm{Pe} < 10^3$ displays a behavior similar to that corresponding to the tent potential [line (a)], while asymptotically (i.e., for large Pe) follows the diffusive scaling $-\mu_R \sim \mathrm{Pe}^{-1}$, as predicted by Eq. (3.13) for $\gamma \to \infty$.

Let us consider the spectral results for the imaginary part $\omega(\varepsilon)$, which are depicted in Fig. 10 for $q=1$ and $q=2$ for different potentials: the ASF and the tent potentials. Numerical spectral results are in perfect agreement with the theoretical scaling Eq. (3.14).

To complete the analysis on parallel flows on the torus, let us consider the case of a velocity field which does not pos-

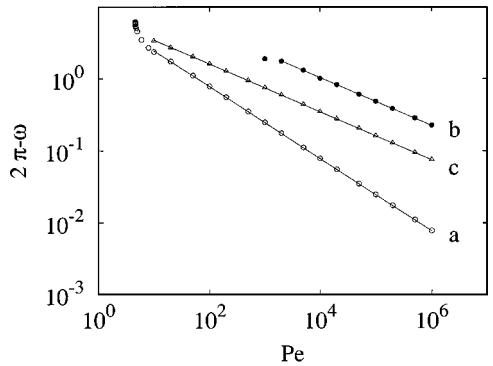

FIG. 10. $2\pi-\omega$ vs Pe. Open circles (○) and filled dots (●) refer to the ASF potential for $q=1$ and $q=2$, respectively. Lines (a) and (b) are the scalings $2\pi-\omega \sim \mathrm{Pe}^{-\alpha}$ with $\alpha=1/2$, $\alpha=1/3$, respectively. Triangles (△) refer to the tent potential Eq. (3.16) with $h=1/4$, and line (c) represents $2\pi-\omega \sim \mathrm{Pe}^{-1/3}$.

sess local maxima/minima and is a smooth monotonic function of x in the open interval (0, 1). Such a potential is manifestly discontinuous at $x=0$ (and $x=1$, since by periodicity these two endpoints coincide). A prototypical model for these class of flows is given by $v_y(x)=x-1/2$. By enforcing the empirical observation that each eigenfunction is localized on a single side of the discontinuity (not shown for the sake of brevity), and applying the same approach based on Eqs. (3.3)–(3.6), it readily follows that for monotonic discontinuous potentials possessing a linear behavior in the neighborhood of the discontinuity, the exponent α is given by

$$\alpha = \frac{1}{2q+1}. \tag{3.17}$$

Equation (3.17) implies that monotonic discontinuous potentials possessing a linear behavior close to the discontinuity falls in the same universality class of the tent potential discussed above, as can be intuitively argued from physical reasons. In the particular case of $q=1$ (Laplacian operator), it follows that $\alpha=1/3$.

D. Eigenvalue multiplicity and symmetries

This section addresses eigenvalue multiplicity and how this is related to the symmetries of the potential. Let us first consider the simple potential belonging to the class analyzed in Sec. III C. We have mentioned that if μ is a complex eigenvalue of $\mathcal{A}_q$, its complex conjugate $\overline{\mu}$ is also an eigenvalue. This property follows from the skew symmetry of the potential $V(1-x)=-V(x)$. To prove this property, let $\psi(x)$ be the eigenfunction associated with μ, and consider the eigenvalue equation for μ, $\psi(x)$,

$$\mathcal{D}\psi(x) + iV(x)\psi(x) = \mu\psi(x), \tag{3.18}$$

where we set $\mathcal{D}=(-1)^{q-1}\varepsilon D_x^{2q}$ for simplifying the notation. By taking the complex conjugate of Eq. (3.18), and making the transformation $x \to 1-x$, it follows that

$$\mathcal{D}\overline{\psi}(1-x) - iV(1-x)\overline{\psi}(1-x) = \overline{\mu}\overline{\psi}(1-x). \tag{3.19}$$

By enforcing the skew symmetry of the potential, and defining $\phi(x)=\overline{\psi}(1-x)$, one obtains

$$\mathcal{D}\phi(x) + iV(x)\phi(x) = \overline{\mu}\phi(x), \tag{3.20}$$

which implies that $\overline{\mu}$ is an eigenvalue of $\mathcal{A}_q$ and $\phi(x)$, defined above, is the eigenfunction associated with this eigenvalue.

Let us now analyze more complex potentials possessing multiple local maxima and minima. The first example is the symmetric potential $V(x)=2\pi\sin(4\pi x)$ displaying two local maxima and two local minima. The spectral plot for $\mathcal{A}_1$ is depicted in Fig. 11(a), and is qualitatively similar to that characterizing the ASF potential [Fig. 2(a)]. There is however an important difference: the dominant eigenvalue μ is twofold symmetric, which implies that there exists four linearly independent eigenfunction associated with eigenvalues possessing the same real part (for the skew-symmetric properties discussed above). Figures 12(a) and 12(b) show the

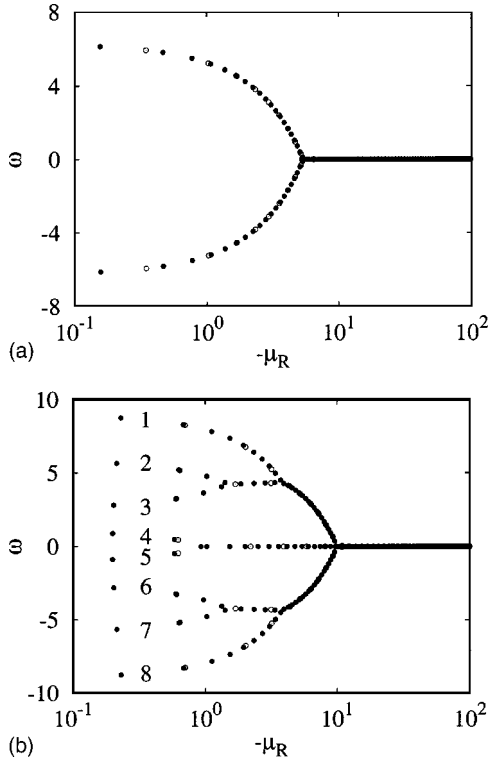

FIG. 11. Spectral plots $-\mu_R$-ω of $\mathcal{A}_q$ for multimaxima potentials. (a) $q=1$, $V(x)=2\pi\sin(4\pi x)$. Open circles (○) refer to Pe$=2\times10^3$, filled dots (●) to Pe$=10^4$. (b) $q=1$, $V(x)=2\pi[\sin(2\pi x)+0.5\sin(8\pi x)]$. Open circles (○) refer to Pe$=5\times10^3$, filled dots (●) to Pe$=10^4$. Labels 1–8 indicate the eightfold branched structure of the complex conjugate eigenvalues.

imaginary part $\psi^I(x)=\mathrm{Im}[\psi(x)]$ of the two degenerate eigenfunctions associated with the dominant eigenvalue.

In the case of more complex potentials, the landscape of which possesses several local maxima/minima of different intensity, many symmetries are broken. This is for example the case of the potential $V(x)$ depicted in Fig. 8(b), the functional expression of which is

$$V(x) = 2\pi[\sin(2\pi x) + 0.5\sin(8\pi x)]. \tag{3.21}$$

The spectral plot of the operator $\mathcal{A}_1$ for this potential is depicted in Fig. 11(b), and is characterized by an eightfold

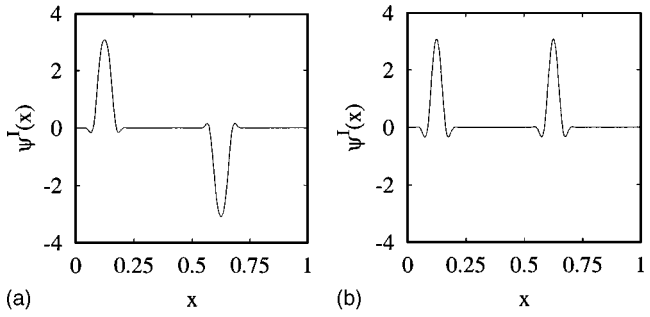

FIG. 12. (a)–(b) Imaginary part of the two dominant degenerate eigenfunctions $\psi^I(x)$ vs x for the operator $\mathcal{A}_1$ associated with the potential $V(x)=2\pi\sin(4\pi x)$ for Pe$=10^4$.

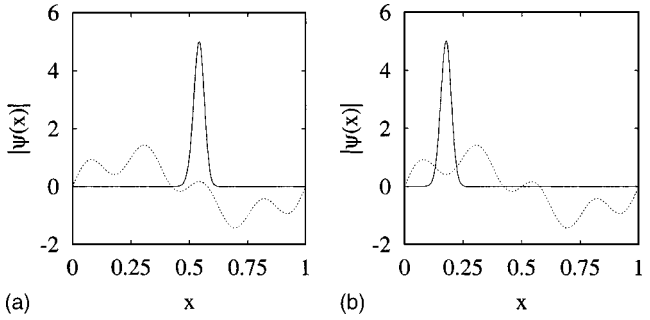

FIG. 13. Modulus $|\psi(x)|$ of the first two dominant eigenfunctions (a) and (b) of the operator $\mathcal{A}_1$ in the presence of the multimaxima potential $V(x)=2\pi[\sin(2\pi x)+0.5\sin(8\pi x)]$ for Pe$=10^4$. The dotted lines in both panels represent the potential $V(x)/2\pi$, drawn in order to highlight the location of its critical points.

branched structure of the complex conjugate eigenvalues, originated by the presence of eight maxima or minima in the potential. Figures 13(a) and 13(b) show the spatial profile of the eigenfunctions for Pe$=10^4$ associated with the first two eigenvalues, the real parts of which are $-\mu_r=0.199$ and $-\mu_R=0.202$. The eigenfunctions are localized around the critical points of the potential, and the scaling of $-\mu_R$ (not shown for the sake of brevity) follows for large Peclet number the universal scaling Eqs. (3.12) and (3.13) with $\gamma=2$.

IV. IMPLICATIONS OF UNIVERSALITY FOR PHYSICALLY REALIZABLE FLOWS

The results obtained in the preceding section for the spectral properties of parallel flows provide a direct physical explanation for the scaling behavior of more complex two-dimensional autonomous flows. This is a consequence of the universality properties characterizing the eigenvalue scaling, that indicates that the exponent α depends exclusively on the behavior of the velocity field near the critical points. It is just because the scaling of the eigenvalues belonging to the convection-enhanced branch of the spectrum depends on the local properties of the velocity field that it is possible to obtain prediction for generic two-dimensional autonomous flows starting from the spectral information obtained for parallel flow models.

The physical reason for this observation stems from the fact that the qualitative behavior of two-dimensional autonomous flows can be locally described by means of a parallel flow model.

To clarify this concept, let us consider two examples. The first is a model flow on the two-dimensional torus (i.e., on the unit square $\mathcal{I}^2$ with opposite edge identified), the stream function of which is given by

$$\Psi(x,y) = -\frac{1-c}{2\pi}\cos(2\pi y) + \frac{1-c}{2\pi}\cos(2\pi x) + \frac{c}{2\pi}\sin(2\pi x)\sin(2\pi y). \tag{4.1}$$

As an illustration, Fig. 14(a) shows the streamline structure for the case where $c=1/2$. The velocity field resulting from

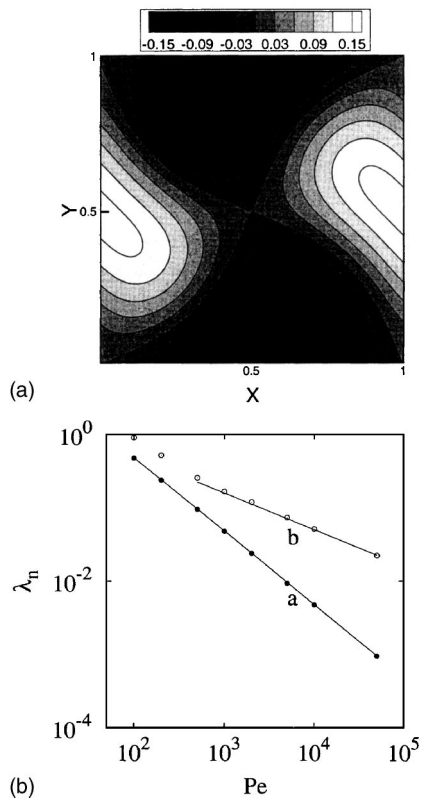

FIG. 14. (a) Contour plot of the stream function Eq. (4.1). (b) Real part with reversed sign λ_n of the dominant eigenvalues of the diffusive (●) and convective (○) branch as a function of Pe for the flow on the torus generated by the stream function Eq. (4.1). Lines (a) and (b) represent the scaling laws $\lambda_n \sim \mathrm{Pe}^{-1}$ and $\lambda_n \sim \mathrm{Pe}^{-1/2}$, respectively.

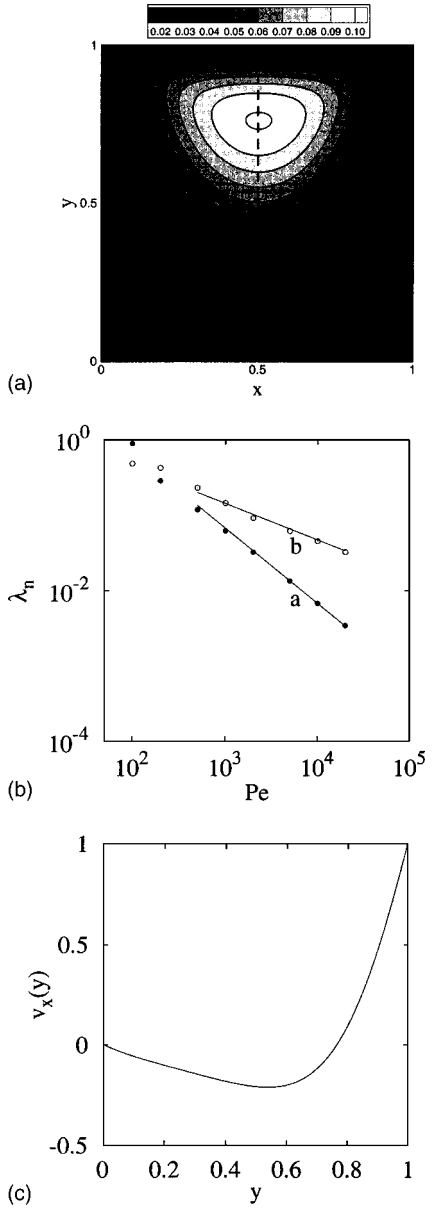

FIG. 15. (a) Contour plot of the stream function for the cavity flow on the unit square in creeping flow regime. (b) Real part with reversed sign λ_n of the dominant eigenvalues of the diffusive (●) and convective (○) branch as a function of Pe for the cavity flow depicted in (a). Lines (a) and (b) represent the scaling laws $\lambda_n \sim \mathrm{Pe}^{-1}$ and $\lambda_n \sim \mathrm{Pe}^{-1/2}$, respectively. (c) $v_x(y)$ at $x=1/2$ for the cavity flow on the unit square.

the stream function is by definition given by $\mathbf{v}(\mathbf{x}) = (\partial\Psi/\partial y, -\partial\Psi/\partial x)$

The second example is the cavity flow in a unit square cavity $\mathcal{Q}^2=\{(x,y)\,|\,0\leqslant x,y\leqslant 1\}$ in the creeping flow regime. We use two different symbols, $\mathcal{Q}^2$ and $\mathcal{I}^2$ to indicate the unit square, since in the latter case, i.e., $\mathcal{I}^2$ the opposite edges are identified, and therefore periodic boundary conditions apply, while for the cavity flow, zero-flux conditions must be enforced at the boundary of the cavity to express the impermeability condition. The stream function Ψ for the creeping cavity flow [Fig. 15(a)] is the solution of the biharmonic equation, $\nabla^4\Psi=0$ with zero velocity at all the edges but at $y=1$, at which $v_x=1$. In terms of Ψ this implies that the tangential derivative along the boundary vanishes together with the normal derivative at the static walls, whereas $\partial\Psi/\partial n=-1$ at $y=1$ along the moving wall.

The solution of the advection-diffusion equation for this flow systems has been obtained by applying a Galerkin expansion with respect to the eigenbasis of the Laplacian operator (see, e.g., [22] for details on the numerical accuracy and on the truncation order).

Both these flows are characterized by the occurrence in the mixing space of recirculation regions: two recirculation regions for the stream function Eq. (4.1) on the torus, delimited by a X-shaped separatrix [see Fig. 14(a)], and a single main recirculation region invading the whole mixing space for the cavity flow [see Fig. 15(a)].

Within each recirculation region one can express the advection-diffusion equation in a new coordinate system, in which one of the coordinates is the stream function itself, and the other coordinate is chosen orthogonal to it (stream-function-based coordinate system). If one expresses the ADE in a stream-function-based orthogonal system, the velocity field possesses solely one nonvanishing component (since it is tangent to the streamlines), analogously to the simple model flows considered in this paper (parallel flows). This can be easily visualized for the square cavity flow, since, by

symmetry, at $x=1/2$, the coordinate line orthogonal to the stream function coincide with the line $x=1/2$ parallel to the y axis. Due to the recirculating structure of the velocity field, the nonvanishing component of the velocity field possesses a nonmonotonic behavior with the occurrence of a single local maximum/minimum. This is clearly depicted in the case of the cavity flow [Fig. 15(c)], which shows $v_x(y)$ along the axis of symmetry $x=1/2$.

By enforcing the universality results obtained for parallel flows, one may expect that the behavior of the nonvanishing velocity fields near its local extremal point influences the scaling behavior of the dominant eigenvalue of the convection-enhanced branch as a function of the Peclet number. Since it is a generic property that smooth functions in a neighborhood of a local extremal point possesses a quadratic nonlinearity, it may be argued that for flow possessing a recirculation region the scaling $\lambda_n \sim \mathrm{Pe}^{-1/2}$ will occur for the convection enhanced branch (apart from a set of flow of zero measure). This prediction is confirmed by direct numerical simulations of the advection-diffusion equations depicted in Figs. 14 and 15(b), which show the dominant eigenvalues of the two branches of the two flow system described above: the diffusional branch, for which $\lambda_n \sim \mathrm{Pe}^{-1}$, and the convection-enhanced branch, for which $\lambda_n \sim \mathrm{Pe}^{-1/2}$, as correctly predicted by the universality theory in the neighborhood of a quadratic nonlinearity.

The same approach discussed above, applies for more complex flow structure possessing more than a single recirculation region, since the analysis developed is of local nature.

It is important to observe that there are physically interesting flow models, which do not possess recirculation regions. For these flows, the velocity component in a stream-function-based coordinate system may be monotonic, and the flow motion is controlled by the topology of the flow domain. A typical example is the two-dimensional creeping flow between two concentric cylinders (two-dimensional Couette flow). For the two-dimensional creeping flow between concentric cylinders possessing radii R_1 and R_2, in which the outer cylinder is moving with velocity ΩR_2, the velocity field in a cylindrical coordinate system (r,θ) possesses solely a nonvanishing component $v_\theta(r)$, given by

$$v_\theta(r) = \Omega r \frac{1-(R_1/r)^2}{1-(R_1/R_2)^2}, \quad R_1 < r < R_2. \tag{4.2}$$

This velocity field is monotonic [see Fig. 16(b), for $R_1=1/2$, $R_2=1$, $\Omega=1$]. The creeping Couette flow is a parallel flow in a cylindrical coordinate system characterized by a monotonic velocity, and the universality theory developed in this paper, see Eq. (3.17), predicts the occurrence of the scaling $\lambda_n \sim \mathrm{Pe}^{-1/3}$, for the convection-enhanced branch. This result is confimed by the direct numerical simulation of the advection-diffusion equation for the creeping flow system, depicted in Fig. 16(a) (these data have been obtained by applying a finite volume algorithm, starting from an initial condition, dependent on the angular variable θ which excites the convection-enhanced branch and possesses vanishing components on the diffusive branch of the eigenspectrum).

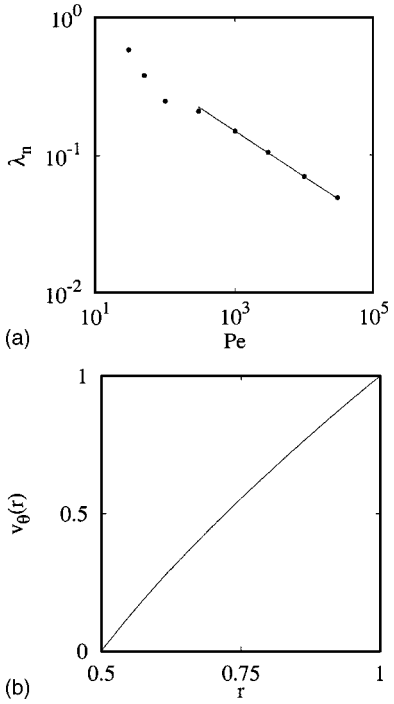

FIG. 16. (a) Real part with reversed sign λ_n of the dominant eigenvalue of and convective branch as a function of Pe for the Couette flow ($R_1=0.5$, $R_2=1$). The solid line is $\lambda_n \sim \mathrm{Pe}^{-1/3}$. (b) Velocity $v_\theta(r)$ vs r for the Couette flow.

The examples and the discussion developed in this section show the practical and physical usefulness of the universality theory developed for parallel flow models for predicting the homogenization/dispersion properties of two-dimensional autonomous flows.

V. CONCLUDING REMARKS

By considering simple model flows Eq. (2.2), we have recast the theoretical analysis of the spectral properties of the advection-diffusion equation in a simpler problem formally analogous to a one-dimensional non-Hermitian Schrödinger equation in the presence of an imaginary potential.

The salient spectral properties of these non-Hermitian operators are (i) spectral invariance; (ii) eigenfunction localization, and (iii) universal eigenvalue scaling. The analysis of the universal scaling leading to Eqs. (3.12) and (3.13) provides a theoretical justification of the observed convection-enhanced behavior occurring in homogenization dynamics in bounded flows, and represents an example of the relationships existing between local properties (the exponent γ) and global spectral features (the exponent α).

The universality theory developed for parallel flows provides a theoretical framework for understanding homogenization properties of more complex flows, as addressed in Sec. IV. While the occurrence of a $\mathrm{Pe}^{-1/2}$ scaling is a generic property characterizing flows possessing recirculation regions, there are physically relevant examples (the creeping Couette flow), for which a different scaling ($\sim \mathrm{Pe}^{-1/3}$) is observed. The theory explains the occurrence of all these cases.

It is remarkable that even the family of operators $\mathcal{A}_q$ possesses a rich spectral structure: complex eigenvalue "spectral arms" coexist with a real branch, giving rise to the forklike spectral plots depicted in Fig. 2. Moreover, the number of complex eigenvalue arms in the absence of specific symmetries is related to the number of critical points (maxima/minima) of the potential.

Equation (3.13) indicates that the "worst" scaling condition $-\mu_R \sim \mathrm{Pe}^{-1}$ is attained in the presence of a potential possessing a flat region, as extensively discussed in connection with the family of potentials Eq. (3.16). Conversely, it may be argued that the "optimal" scaling condition $\mu_R \sim$ constant for $\mathrm{Pe} \to \infty$ may be achieved by considering continuous but locally nondifferentiable potentials possessing cusplike local maxima. Whether and how the latter observation can be related to fluid dynamics, is an open problem.

Beyond the relatively straightforward analogy between the advection-diffusion equation, and a class of non-Hermitian Schrödinger-type operators [the family of operators $\mathcal{A}_q$ Eq. (2.9), and specifically $\mathcal{A}_1$], an intriguing issue is whether and how this analogy could be pushed further, especially in the presence of more complex velocity fields giving rise to a partially chaotic condition. This is an open question, that could have important conceptual implications in the characterization of quantum chaos, and in the analysis of the semiclassical limit of quantum mechanics.

[1] G. T. Csanady, *Turbulent Diffusion in the Environment* (Reidel, Dordrecht, 1973).

[2] J. Baldyga and J. R. Bourne, *Turbulent Mixing and Chemical Reaction* (Wiley, Chichester, 1999).

[3] J. Villermaux, Rev. Chem. Eng. **7**, 51 (1991).

[4] G. K. Batchelor, J. Fluid Mech. **1**, 177 (1956).

[5] P. Castiglione, A. Mazzino, P. Muratore-Gianneschi, and A. Vulpiani, Physica D **134**, 75 (1999).

[6] T. Tel, G. Karolyi, A. Pentek, I. Sheuring, Z. Toroczkai, C. Grebogi, and J. Kadtke, Chaos **10**, 89 (2000).

[7] M. Giona, S. Cerbelli, and A. Adrover, J. Phys. Chem. **106**, 5722 (2002).

[8] S. Cerbelli, A. Adrover, and M. Giona, Phys. Lett. A **312**, 355 (2003).

[9] V. Toussaint, P. Carriere, and F. Raynal, Phys. Fluids **7**, 2587 (1995).

[10] V. Toussaint, P. Carriere, J. Scott, and J.-N. Gence, Phys. Fluids **12**, 2834 (2000).

[11] A. Fannjiang and G. Papanicolaou, SIAM (Soc. Ind. Appl. Math.) J. Appl. Math. **54**, 333 (1994).

[12] S. Childress and A. M. Soward, J. Fluid Mech. **205**, 99 (1989).

[13] A. Bensoussan, J.-L. Lions, and G. Papanicolau, *Asymptotic Analysis for Periodic Structures* (North-Holland, Amsterdam, 1978).

[14] S. Agmon, *Lectures on Elliptic Boundary Value Problems* (Van Nostrand, Princeton, 1965).

[15] M. Faierman, "On the spectral theory of an elliptic boundary value problem involving an indefinite weight," in *Operator Theory and Boundary Eigenvalue Problems*, edited by I. Gohberg and H. Langer (Birkhäuser Verlag, Basel, 1995), pp. 137–154.

[16] M. Liu, F.J. Muzzio, and R.L. Peskin, Chaos, Solitons Fractals **4**, 869 (1994).

[17] M. M. Alvarez, F. J. Muzzio, S. Cerbelli, A. Adrover, and M. Giona, Phys. Rev. Lett. **81**, 3395 (1998).

[18] L. Prandl and O. G. Tietjens, *Fundamentals of Hydro- and Aeromechanics* (Dover, New York, 1957).

[19] N. Hatano and D. R. Nelson, Phys. Rev. Lett. **77**, 570 (1996).

[20] N. Hatano and D. R. Nelson, Phys. Rev. B **56**, 8651 (1997).

[21] I. Ya. Goldsheid and B. Khoruzhenko, Electron. J. Probab. **5** (paper no. 16), 1 (2000).

[22] A. Adrover, S. Cerbelli, and M. Giona, Comput. Chem. Eng. **26**, 125 (2002).